Ba$_x$Sr$_{1-x}$Ti$_{1.02}$O$_3$ metal–insulator–metal capacitors on planarized alumina substrates

M.P.J. Tiggelman [a],[*], K. Reimann [b], M. Klee [c], R. Mauczock [c], W. Keur [c], R.J.E. Hueting [a]

[a] MESA+ Institute for Nanotechnology, Chair of Semiconductor Components, University of Twente, 7500 AE Enschede, The Netherlands
[b] NXP Semiconductors, Corporate I &T/Research, 5656 AE Eindhoven, The Netherlands
[c] Philips Research Laboratories, 5656 AE Eindhoven, The Netherlands

ARTICLE INFO

ABSTRACT

Nanocrystalline barium strontium titanate (Ba$_x$Sr$_{1-x}$Ti$_{1.02}$O$_3$) thin films with a barium content of $x = 0.8$, 0.9 and 1 have been fabricated in a metal–insulator–metal configuration on glass-planarized alumina substrates. Cost-effective processing measures have been utilized by using poly-crystalline alumina substrates, wet-chemical processing of the dielectric, and by a small physical area of the ferroelectric capacitors (as low as 50 μm^2 for radio frequencies measurements). Glass-planarization on alumina ceramic substrates enables barium strontium titanate films with high quality and homogeneity. We mainly focus on fine-tuning the electrical performance in the low gigahertz range (<10 GHz). Extensive micro-structural and electrical characterization has been performed. Micro-structural information is obtained by: Transmission Electron Microscopy, Scanning Electron Microscopy and X-ray diffraction. The dielectric response is investigated as a function of temperature, frequency and electric field for each sample. We measured a relatively constant permittivity for typical operating temperatures of applications. The quality factor Q is between 21 and 27 at 1 GHz at zero DC bias and the tuning ratio η between 1.8 and 2.2 at $|E| = 0.4$ MV/cm.

Crown Copyright © 2009 Published by Elsevier B.V. All rights reserved.

1. Introduction

The integration of an increasing amount of functionality in handheld applications in combination with the miniaturization of electronic circuitry is challenging. Reconfigurable capacitor components in microwave applications such as Micro Electro-Mechanical Systems capacitor switches [1], varactor diodes [2] or solid-state tunable ferroelectrics [3] can facilitate this trend. Non-linear thin film ferroelectric capacitors in the paraelectric phase [4] are attractive for radio frequency (RF) passive integration due to a low loss tangent, high permittivity ($\varepsilon_r = 100$–1000), tuning at relatively low voltages (typically <40 V$_{dc}$), high tuning ratio (>2:1), small area consumption ($A < 60$ μm^2), and integrated decoupling [5].

Over the years various ferroelectric materials [6,7] have been investigated for microwave applications, e.g., Bi$_{1.5}$Zn$_{1.0}$Nb$_{1.5}$O$_7$ [8], (Pb, Zr)TiO$_3$ [9], and Ba$_x$Sr$_{1-x}$Ti$_y$O$_3$ (BST) [10–12]. Barium strontium titanate (BST) has obtained considerable attention by research groups worldwide and can be grown on single crystal substrates, e.g., sapphire, magnesium oxide, yttrium barium copper oxide, strontium titanate, or lanthanum aluminate, at high temperatures. However, single crystal substrates are rather expensive.

To achieve low-cost devices, several groups are investigating the use of ceramic Al$_2$O$_3$ substrates as carrier. Ceramic Al$_2$O$_3$ substrates are also attractive due to the excellent match of the thermal expansion coefficient with BST [13]. Elevated processing temperatures cause less strain, which can affect the electrical performance [13–15].

Unpolished ceramic substrates are, however, very rough and give rise to short circuited capacitors. Therefore capacitors on top of either polished ceramic substrates or substrates with planarization layers [13] are studied. BST processed by RF sputtering on top of polished alumina substrates was intensively studied by Nath et al. [16] and Ghosh et al. [17]. Deposition of BST metal–organic decomposition on alumina substrates with planarization layer is reported by Koutsaroff et al. [13] for integrated multilayer capacitors.

In this paper we discuss the micro-structural growth as well as low and radio frequency properties of BST thin film of various compositions. In order to realize high performance devices at low cost for reconfigurable RF applications, the growth and properties for thin BST films on poly-crystalline Al$_2$O$_3$ (alumina) with a planarization layer has been studied. The structural characterization has been carried out by Scanning Electron Microscopy (SEM), a Transmission Electron Microscopy (TEM), and by X-ray diffraction (XRD) analysis in Section 2. Furthermore, the dielectric response is investigated as a function of temperature, frequency and electric field for each sample. In Section 3 we discuss the material analysis and the measurement results. The conclusions are listed in Section 4.

* Corresponding author.
E-mail address: m.p.j.tiggelman@utwente.nl (M.P.J. Tiggelman).

2. Processing and characterization

2.1. Sample fabrication

$Ba_xSr_{1-x}TiO_3$ (BST) solutions with $x = 0.8$, 0.9 and 1.0 have been deposited using wet-chemical processing on commercially available alumina substrates, which comprised a glass-planarization layer. Solutions with a $(Ba + Sr)$:Ti ratio of 1.00:1.02 were used. We also investigated a limited number of samples with the stoichiometric composition, with the $(Ba + Sr)$:Ti ratio of 1.00:1.00. The electrical data show no significant difference to the samples with the Ti excess. We therefore report only the data for the samples with Ti excess. We applied solutions with a slight Ti excess to reliably prevent Ba excess in all films, which could result in a strong sensitivity to moisture. On top of the planarization layer two layers are deposited by sputtering: a thin titanium (Ti) layer of 10 nm, and a platinum (Pt) layer of 140 nm which forms a homogeneous bottom electrode. The BST layers were deposited by spin-on using a modified sol–gel solution. For the BST the precursors barium and strontium acetates were dissolved in acetic acid. The alkaline earth solution is added to a titanium alkoxide solution, which is formed from titanium iso-propoxide with 1-methoxy-2-propanol as solvent. The spin-on solutions developed here have a long term stability of more than 3 months, which was confirmed by reproducibility measurements of dielectric thickness and capacitance density. Films were spin-coated and the solvent is evaporated on a hot-plate at 150–250 °C for 1–3 min. Crystallization is carried out at a temperature of 700 °C for all samples. As a top electrode for the capacitors Pt(100 nm)/Au(500 nm) is applied. For the electrical device characterization only the top electrode is patterned [18] using dry etching procedures.

2.2. Micro-structural characterization

Information on the micro-structure is obtained by three material characterization methods: SEM, TEM and XRD. In Fig. 1 X-ray diffraction patterns of all compositions discussed in this paper were shown. The BST grows in a single-phase and randomly oriented on top of the Pt{111} electrodes.

A dielectric thickness of 530 nm ± 12 nm is measured for our devices by SEM images obtained from a Philips SEM XL40 FEG. TEM samples were prepared using a FIB200 (FIB stands for Focussed Ion Beam). Before FIB preparation, a thin Pt layer is deposited in a sputter coater to avoid charging on the entire sample. After this deposition a 1.5 μm Pt layer is deposited in the FIB on the region of interest to protect the sample during FIB milling. As a final cleaning step, a 5 kV milling step was performed on the Nova Nanolab200 small dual beam.
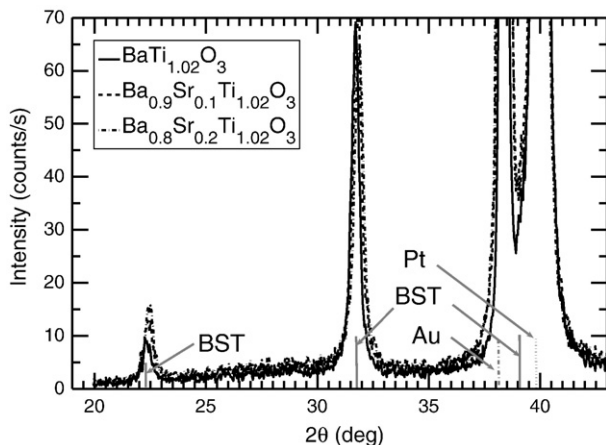
TEM studies were performed using a TECNAI F30ST TEM operated at 300 kV.

The grain size, obtained with TEM, was measured using dark-field images (see Fig. 2). The grain size is determined by averaging over 160–230 grains with one crystallographic orientation for each sample (see the light grains in the dark-field image in Fig. 2). The XRD measurements have been performed with a PANalytical X'Pert Pro MPD diffractometer, equipped with a Cu X-ray source. The grain sizes by XRD were determined from the broadening of the {110} line of a θ–2θ scan, which yields an average diameter normal to the substrate. The {110} reflection of each sample was fitted by a Voigt function (convolution of a Gaussian and a Lorentz function [19]) and the grain size was calculated from the half-width (Scherrer's formula [20]) or integral width of the peak, which gives the volume weighted diameter $\langle D \rangle_v$ [21]. The difference of both values is a measure for the spread in the distribution of crystallite sizes. The relatively small difference (see Table 1) indicates a narrow distribution, as also shown by the TEM results.

Wide-angle X-ray diffraction measurements of samples that were processed similarly indicated that microstrains (strain variations) have only a minor influence on the X-ray line broadening, so that the Scherrer analysis can be employed for estimating the crystallite size. X-ray and TEM results were in good agreement. We derive from these data that our thin BST films have been growing on top of alumina substrates with planarization layer and are extremely fine-grained. The grain sizes were in the order of 20–24 nm. We do not observe strong differences in grain size for BST films processed at the same processing temperature. All three methods indicate, that with increasing strontium content in the BST films with excess titanium, there is a slight decrease of the grain size by 10%.

Our thin films grown on alumina substrates with planarization layer grown at 700 °C show comparable grain size of 49 nm to BST films with 30 at.% strontium grown on alumina with planarization layer processed by metal–organic deposition at temperatures of 685 °C reported by Koutsaroff et al.[22]. Ioachim et al. [23] processed BST with 50 at.% strontium by pulsed laser deposition on sapphire and alumina substrates. To improve granular growth doping with MgO and MnO_2 is applied [24]. These BST films were also annealed at high temperatures of 800 °C and show grain sizes of 50–60 nm.
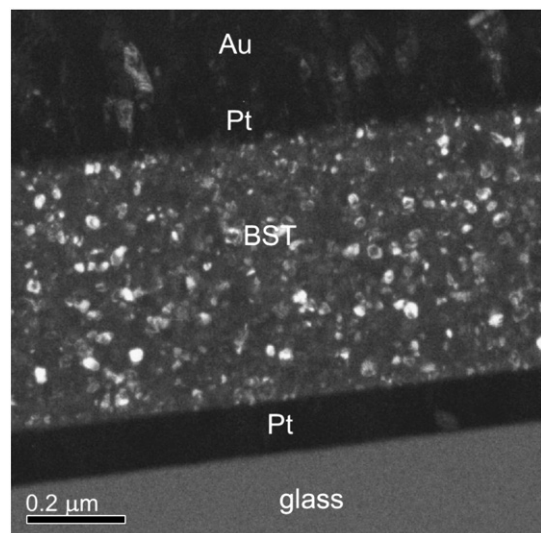

Fig. 2. A dark-field TEM cross-section of a metal–insulator–metal (MIM) capacitor is visualized on top of a smooth glass-planarization layer and an alumina substrate (not depicted). The Ti layer below the Pt bottom electrode is too thin to be visible. The poly-crystalline structure of the $Ba_{0.9}Sr_{0.1}Ti_{1.02}O_3$ is clearly visible. The grain size is averaged over 160–230 grains with one crystallographic orientation (see the light colored grains).

Fig. 1. X-ray patterns of the reported compositions on alumina.

Table 1
The grain size with XRD is determined using Scherrer's formula, the integral width of the peak, which results in the volume weighted diameter $\langle D \rangle_v$, and by a TEM analysis.

BST composition	Scherrer {110}	$\langle D \rangle_v$	TEM
$BaTi_{1.02}O_3$	22.4 ± 0.6 nm	23.5 ± 0.4 nm	23 ± 14 nm
$Ba_{0.9}Sr_{0.1}Ti_{1.02}O_3$	20.4 ± 0.5 nm	21.1 ± 0.4 nm	21 ± 11 nm
$Ba_{0.8}Sr_{0.2}Ti_{1.02}O_3$	19.7 ± 0.6 nm	20.2 ± 0.4 nm	18 ± 6 nm

The deviations ($\pm$) for XRD indicate statistical accuracy of the mean value, not the width of the crystallite size distribution. The deviations for TEM were caused by the large standard deviation of the grain size. The accuracy from the mean from the TEM image can be determined by dividing the standard deviation by $\sqrt{n+1}$, with n the number of grains.

2.3. Electrical characterization

The electrical characterization of our BST thin films is split up in three parts: temperature, frequency, and electric field response of the MIM capacitors.

2.3.1. Temperature response

Temperature sweeps were performed using a Novocontrol Quatro cryostat with a BDS1100 sample holder and a HP4192 Impedance Analyzer. Ring shaped MIM capacitors with an area of about 275,000 μm^2, of which only the top electrode is patterned, have been measured at zero DC bias and an AC voltage of 0.1 V_{ac}. The measurement frequency of 100 kHz is low enough to avoid electrode and contact resistance influence (shown by an increase in tanδ) and is sufficiently high to perform accurate capacitance measurements (the impedance of the small capacitors becomes very high). A temperature sweep has been performed from $-160\,°C$ to $180\,°C$. The ε_r of all BST compositions in response to the temperature sweep is shown in Fig. 3.

The BST thin films show a broad permittivity plateau $T_{\varepsilon_r,max}$ at the Curie temperature (see Fig. 3). For the barium titanate films without strontium content the temperature at the maximum relative permittivity has been determined to be 45–50 °C. The relative permittivity is 420 at 21 °C, 100 kHz for the $BaTi_{1.02}O_3$ samples. For our BST films with 10 and 20 at.% strontium, processed with 2% Ti excess, the maximum relative permittivity was shifted from 40 °C for the barium titanate film to 20 °C and $-20\,°C$, which corresponds with a shift of the broad Curie temperature of 3–4 °C/at.% strontium [25].

Over the temperature range from $-55\,°C$ up to 125 °C the relatively permittivity of the $BaTi_{1.02}O_3$ and the $Ba_{0.9}Sr_{0.1}Ti_{1.02}O_3$ samples change less than $\pm 15\%$, and therefore meet the so called X7R specification. The maximum permittivity is shifted with Ba content (see Fig. 4), as known from single crystal data and bulk ceramics (see Fig. 30 in [4] and [10]). Fig. 3 shows that the Curie maximum is broadened for all thin films and
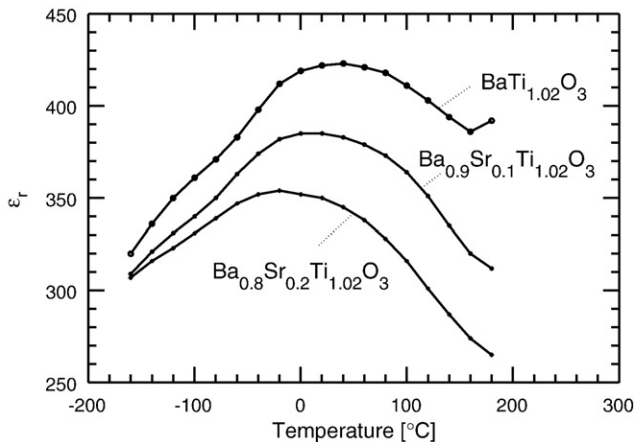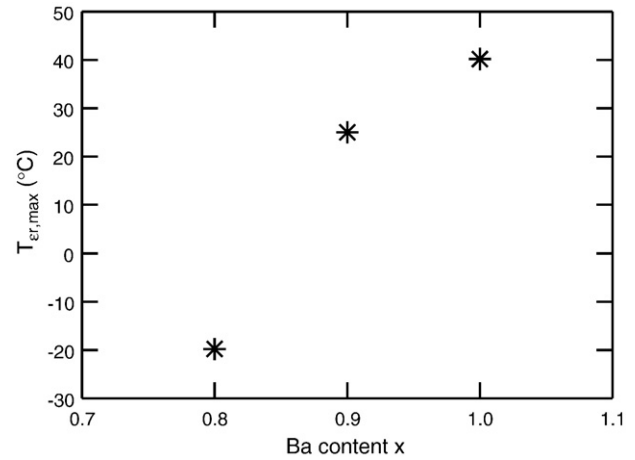
Fig. 4. The temperature at which the permittivity peaks for the BST samples on alumina. The samples were measured on an area $A = 275,000\ \mu m^2$ at 100 kHz, zero DC bias, and 0.1 V_{ac} AC voltage.

the maximum value is lower compared to the value of the related bulk ceramics. This is also reported by other groups [26,27]. These effects were explained by Parker et al. [26] by interface layers with reduced permittivity and Curie temperature. Thomas et al. [27] discuss small grain size effects along with the interaction of grains via depolarization field, stress from the substrate, elastic strain, and thermal fluctuations that can mask the measurable properties at the transitions resulting in such suppression.

The loss tangent with temperature is depicted in Fig. 5. For all BST thin films with barium content of 80–100 at.%, with titanium excess, a loss tangent of 1.1–2.1% up to a 100 °C is measured, where the lowest loss tangent is obtained for the BST film with 80 at.% Ba. The loss tangent is essentially constant across the full temperature range and especially in the application range from $-50\,°C$ to 100 °C. No peak as with bulk ceramics is obtained due to the very fine-grained (20–25 nm) poly-crystalline BST thin films.

2.3.2. Frequency response

To study the performance of our BST thin films for various applications, frequency sweeps have been performed up to 8 GHz. At low frequencies an HP4194a impedance analyzer is used, up to 5 MHz, to obtain the dielectric properties such as permittivity (see Fig. 6) and loss tangent (see Fig. 7) at 50 mV_{ac} AC voltage.

Relaxation effects decrease the permittivity linearly on a logarithmic frequency scale according to the Curie–von Schweidler law [28–30].
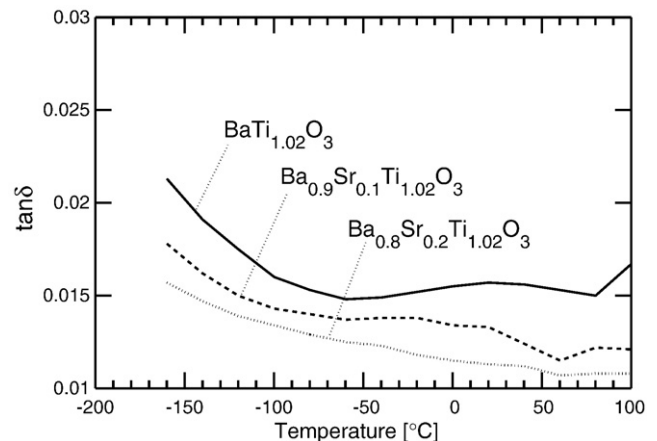
Fig. 3. The change in permittivity with an increase in temperature for BST samples on alumina measured on an area $A = 2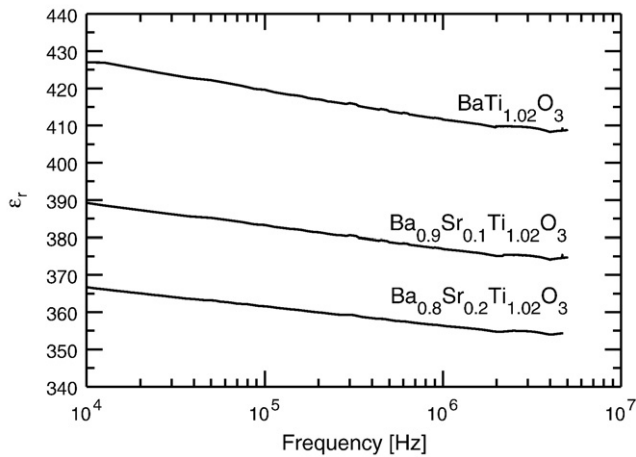75,000\ \mu m^2$ at 100 kHz, zero DC bias, and 0.1 V_{ac}. A decrease in barium content in BST shifts and reduces the peak of the ε_r.

Fig. 5. The change in tan δ with an increase in temperature of all BST samples on alumina measured on an area $A = 275,000\ \mu m^2$ at 100 kHz, zero DC bias, and 0.1 V_{ac}.

Fig. 6. The permittivity of BST compositions measured on 250 µm × 250 µm capacitors at zero DC bias, ambient temperature and 50 mV$_{ac}$ AC voltage.

Fig. 8. The ε_r with frequency of all samples across 8 orders of magnitude obtained with an impedance analyzer (250 µm × 250 µm capacitors measured at 50 mV$_{ac}$, zero DC bias and at an ambient temperature) and with a VNA (circular capacitors with a signal pad diameter of $d = 88$ µm and $d = 8$ µm were measured at −10 dBm RF power, zero DC bias and at an ambient temperature).

The loss tangent of 250 µm × 250 µm capacitors is measured at zero DC bias, ambient temperature and 50 mV$_{ac}$ AC voltage. For the pure BaTiO$_3$ film losses of 2% at 100 kHz and ambient temperature were determined. The BaTiO$_3$ films with Ti excess shows a slightly lower loss of 1.5%. The BST films with strontium content of 10–20% show lower Curie temperatures than the pure BST films and lower losses of 1.0% (see Fig. 7).

Radio frequency measurements have been performed with an Advantest R3767CG vector network analyzer from 500 kHz up to 8 GHz. The RF test structures have a top electrode area size as low as 50 µm². Circular shaped ground–signal–ground (GSG) structures were employed for the RF measurements as discussed in [31]. Cascade Microtech GSG probes were used with a pitch of a 125 µm. The radio frequency response was measured at an RF power of −10 dBm, zero DC bias, and at room temperature. A wide-band frequency analysis was measured with an impedance analyzer and a VNA and combined in a single plot. The relative permittivity and the loss tangent, across 8 orders of magnitude, are depicted in respectively Figs. 8 and 9.

To minimize the noise, a relatively large capacitor was taken with an area of 250 µm × 250 µm at LF, and a large capacitor at RF with a signal pad diameter of 88 µm. Capacitors with a small signal pad diameter of 8 µm were used to reduce the influence of the electrical losses due to the electrodes [31].

In Fig. 9 the loss tangent from a 250 µm × 250 µm BaTi$_{1.02}$O$_3$ MIM capacitor of the impedance analyzer, and from circular RF test structures
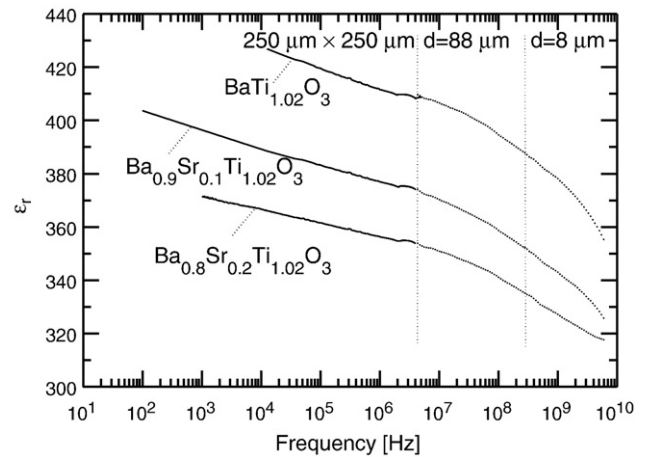
with a diameter $d = 88$, 24, and 8 µm were given. Smaller capacitances were used at higher frequencies to minimize the loss added by the electrodes. The tanδ was relatively flat around 1.4% up to almost 100 MHz, and below 5% up to 1 GHz. In the gigahertz range the losses increase due to the electrodes.

The quality factor of the dielectric with the electrodes is expressed by

$$Q = \frac{1}{\tan\delta} \tag{1}$$

with Q the reciprocal of the loss tangent tanδ. The Q is investigated at 1 GHz, zero DC bias, −10 dBm RF power and at an ambient temperature. Capacitors with a signal pad diameter of 8 µm have been measured at an ambient temperature and at zero DC bias. The Q as a function of barium content in the BST thin films is depicted in Fig. 10. At 1 GHz the BST films, grown on planarized alumina substrates and processed under same processing conditions, show quality factors of 21 for BaTi$_{1.02}$O$_3$, 25.5 for BST with 90 at.% Ba, and 27 for BST with 80 at.% Ba. These measured data are comparable to data reported in literature for sputtered and chemical surface deposition deposited BST MIM capacitors with 70 at.% Ba,
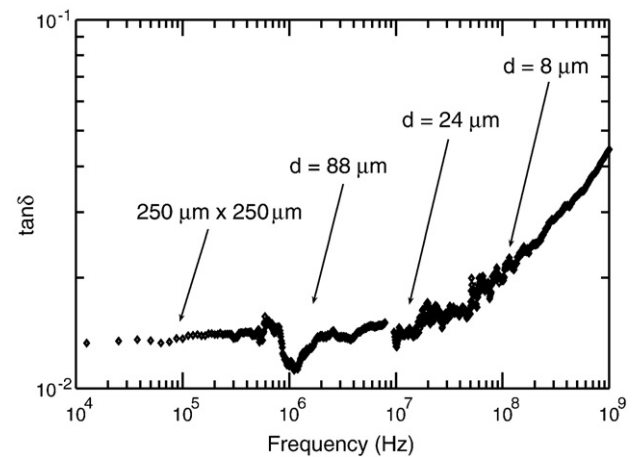

Fig. 7. The loss tangent of a 250 µm × 250 µm capacitor measured at zero DC bias, ambient temperature and 50 mV$_{ac}$ AC voltage.

Fig. 9. The broadband frequency response of tanδ of a relatively large 250 µm × 250 µm BaTi$_{1.02}$O$_3$ MIM capacitor, measured on an impedance analyzer at 50 mV$_{ac}$, and circular RF circular DUTs with a diameter $d = 88$, 24 and 8 µm were measured on a VNA at −10 dBm RF power, zero DC bias and at an ambient temperature.
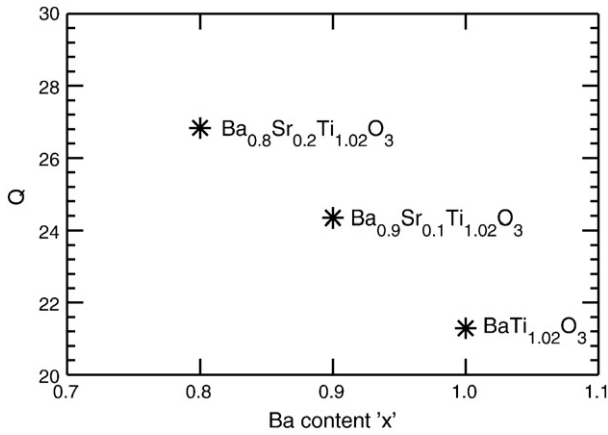
Fig. 10. The quality factor at 1 GHz performed on circular ground–signal–ground RF structures with a signal pad diameter of 8 μm for the reported at − 10 dBm, zero DC bias and at an ambient temperature.

processed on alumina substrates with SiO_2 layer. Koutsaroff et al. [32] report quality factors of 20–30 at 1 GHz.

Our results show that BST thin films grown on top of alumina substrates with glass-planarization layer can be processed poly-crystalline with relative permittivities of 350–420, where the films with the highest relative permittivity show the lowest quality factor. Note that the quality factor at 1 GHz changes less than 50% when the composition is varied between 80 and 100 at.% Ba. It is expected that the Q-factor will increase even further for even lower Ba content, when the Curie temperature is shifted below the operating temperature [10].

2.3.3. Electric field response

The most commonly-used stimulus to tune the permittivity of a ferroelectric material is an electric field E. DC voltage sweeps were performed on a probe station with an HP4194a impedance analyzer. Accordingly, the DC voltage is superimposed with the AC voltage and a tunable capacitor can be measured. 100 μm × 100 μm and 250 μm × 250 μm test structures were measured during an upwards DC voltage sweep at 1 MHz and 50 mV_{ac} AC voltage. A positive DC voltage is applied on the top electrode with the bottom electrode at 0 V. The tuning of the permittivity with electric field in Fig. 11 is limited by the measurement equipment to $|E| = 0.4$ MV/cm. The zero DC bias permittivity is determined by the dielectric composition and the
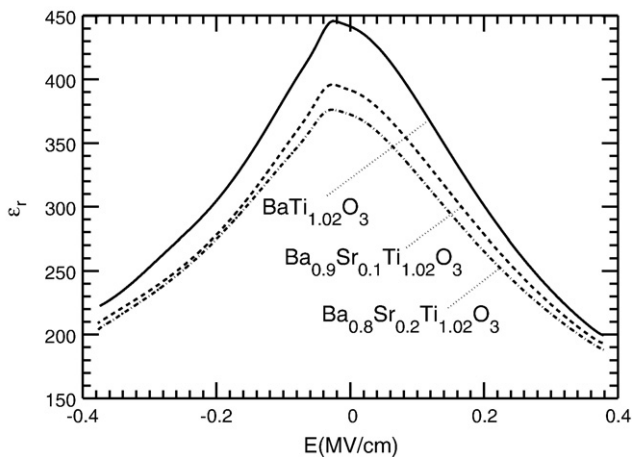

Fig. 11. The ε_r with an electric field of the BST samples on alumina during an upwards DC voltage sweep. The 100 μm × 100 μm test structures have been measured at 1 MHz, 50 mV_{ac} and at an ambient temperature. The permittivity decreases with a lower amount of barium and with increasing absolute electric field.
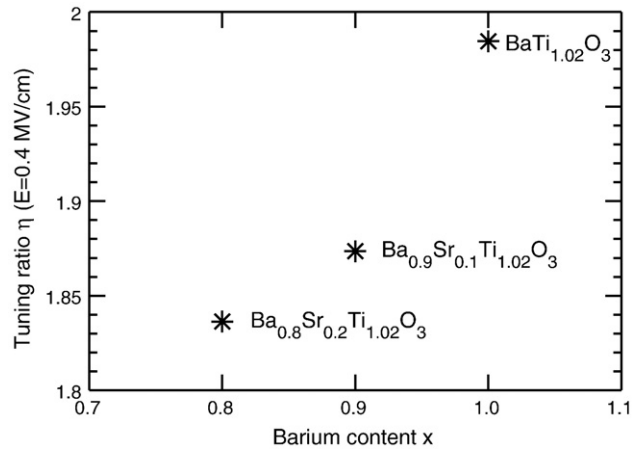

Fig. 12. The tuning ratio at an electric field of at $E = 0.4$ MV/cm in relation to the amount of Ba in $Ba_xSr_{1-x}Ti_{1.02}O_3$ at 1 MHz, at an ambient temperature, and an AC voltage of 50 mV_{ac}.

processing. The closer the operating temperature is to T_c, the larger the permittivity (see Figs. 3 and 11).

The tuning ratio, at a specified electric field E, is expressed as

$$\eta = \frac{\varepsilon_r(0\,\text{MV}/\text{cm})}{\varepsilon_r(E)} \qquad (2)$$

The relationship between the permittivity at zero DC bias and the tuning ratio at 0.4 MV/cm (20 V_{dc}) is shown in Fig. 12 for all compositions.

The tuning ratio η ($E = 0.4$ MV/cm) is between 1.8 (low barium content in BST) and 2.0 (high barium content in BST).

All samples were mainly in the paraelectric phase (ambient temperature > T_c), and have reduced hysteresis effects, a lower permittivity and loss tangent (see the tanδ in Fig. 13). An example of minor hysteresis is seen in the inset of Fig. 13 in which a measured upwards and downwards $C_s(V)$ sweep of a $Ba_{0.9}Sr_{0.1}Ti_{1.02}O_3$ sample is shown.

3. Discussion

In this paper BST thin films with various compositions with 80–100 at.% Ba and no or slight Ti excess of only 2% were processed on top of alumina substrates with a glass-planarization layer. The effects on the micro-structure and electrical parameters with temperature, frequency and electric field in a parallel plate configuration were studied. An overview of the material analysis and the measurement results is given in Table 2 for the samples with Ti excess.
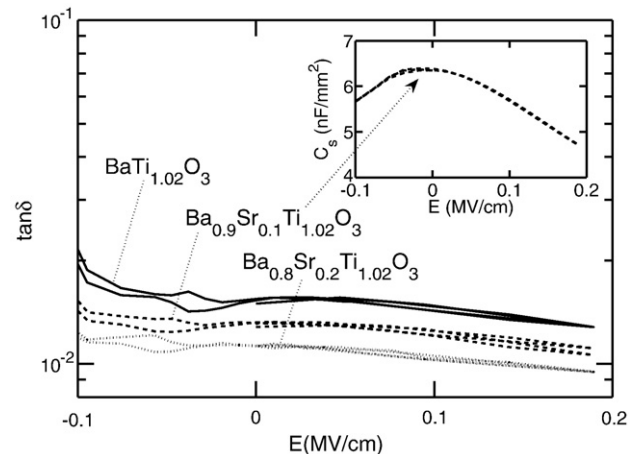

Fig. 13. The loss tangent of BST on alumina of the samples measured at 100 kHz at an ambient temperature in the cryostat.

Table 2
An overview of the material analysis and measurement results of the reported BST samples.

$Ba_xSr_{1-x}Ti_{1.02}O_3$	$\langle D \rangle_S$ {110} [nm]	T_{max} [°C]	ε_r (21 °C)	$\tan\delta_+$ max (100 kHz) [%]	η (E_1)	Q (1 GHz)
$x = 1.0$	22.4	45	420	1.6	2.0	21
$x = 0.9$	20.4	20	383	1.3	1.9	24
$x = 0.8$	19.7	−20	362	1.1	1.8	27

x : composition of $Ba_xSr_{1-x}Ti_{1.02}O_3$.
$\langle D \rangle_S$: crystallite size according to the Scherrer analysis of the {110} reflection.
T_{max} : temperature that maximizes ε_r.
ε_r : dielectric permittivity, measured at an ambient
       : temperature, 0 V_{dc}, 100 kHz and 50 mV_{ac}.
$\tan\delta_+$: maximum loss tangent at 100 kHz for positive E.
E_1 : sample field strength: $E_1 = +0.4$ MV/cm.
η : tuning ratio.
Q : quality factor at 0 V, 1 GHz and −10 dBm.

BST thin film MIM capacitors processed on alumina substrates with glass-planarization deposited by spin-on conditions at low temperatures of 700 °C grow extremely fine-grained with grain sizes of 19.7–22.4 nm. The $BaTi_{1.02}O_3$ film shows the largest grain size of 22.4 nm, although the grain size only depends weakly on the composition. The $BaTi_{1.02}O_3$ film shows the highest relative permittivity of 420 at 21 °C and 100 kHz. This goes along with the highest tunability of 2.0 at 0.4 MV/cm and 1 MHz. With increasing strontium content in the BST films a slight decrease of the grain size is obtained and a decrease of permittivity is measured (see Fig. 6). The BST films with 0–20 at.% strontium show a linear decrease of the relative permittivity from 420 to 362 with increasing strontium content, which goes along with a decrease in the tunability from 2.0 to 1.8, and an increase of the quality factor from 21 to 27 at 1 GHz. The highest Q is obtained for the 20 at.% strontium BST film, whereas the $BaTi_{1.02}O_3$ films show slightly lower values of 21. The decrease of the Q as function of strontium content is also observed for BST single crystals by Bethe [10] and attributed to anharmonic–thermionic 3-phonon atten-uation. For poly-crystalline films that are in the paraelectric phase: the closer the operating temperature to the Curie temperature, the higher the ferroelectric contribution resulting in a higher loss tangent. Comparing our thin BST film data on planarized alumina with data reported in literature, Koutsaroff et al. [32] reports for RF sputtered 100 nm thick BST plate capacitors on alumina substrates with an SiO_2 buffer layer a Q of 20 at 1 GHz. Furthermore, Ghosh et al. [17] reports a Q of 30 at 26 GHz for BST capacitors on polished alumina. For BST thin films with a tuning range of 1.8–2.2 and a Q of 21–27 at 1 GHz these MIM capacitors consist of small dimensions, were processed on a low-cost substrate and are considered for microwave frequency agile applications such as adaptive antenna impedance matching circuits in mobile applications.

4. Conclusion

530 nm thick poly-crystalline $Ba_xSr_{1-x}Ti_{1.02}O_3$ MIM capacitors, on glass-planarized alumina substrates, with a barium content $x = 0.8$–1.0 have been investigated using micro-structural and electrical characterization. More barium content in BST results in an increase of $T_{(\varepsilon_{max})}$ and grain size, which leads to a higher permittivity, and a higher tuning ratio at the cost of the quality factor. The changes in the BST composition resulted in a tuning ratio η between 1.8 and 2.0 at $|E| = 0.4$ MV/cm, and a Q of 27–21 at 1 GHz at

zero bias. The devices processed on low-cost alumina substrates with planarization layers have resulted in a good performance of tunable ferroelectric capacitors, which are considered for microwave appli-cations such as adaptive matching circuits.

Acknowledgements

References

[1] T.G.S.M. Rijks, P.G. Steeneken, J.T.M. van Beek, M.J.E Ulenaers, A. Jourdain, H.A.C. Tilmans, J. de Coster, R. Puers, J. Micromechanics Microengineering 16 (2006) 601.
[2] C. Huang, L.C.N. de Vreede, F. Sarubbi, M. Popadic, K. Buisman, J. Qureshi, M. Marchetti, A. Akhnough, T.L.M. Scholtes, L.E. Larson, L.K. Nanver, IEEE Trans. Microwave Theor. Tech. 56 (2008) 1149.
[3] M. Klee, H. van Esch, W. Keur, B. Kumar, L. van Leuken-Peters, J. Liu, R. Mauczok, K. Neumann, K. Reimann, C. Renders, A.L. Roest, M.P.J. Tiggelman, M. de Wild, O. Wunnicke, J. Zhao, IEEE Trans. Ultrason. Ferroelectr. Freq. Control 56 (2009) 1505.
[4] A.K. Tagantsev, V.O. Sherman, K.F. Astafiev, J. Venkatesh, N. Setter, J. Electroceramics 11 (2003) 5.
[5] M. Klee, P. Löbl, R. Kiewitt, W. Brand, P. van Oppen, P. Lok, Mater. Res. Soc. Symp. Proc. 596 (2000) CC13.1.1.
[6] S.S. Gevorgian, E.L. Kollberg, IEEE Trans. Microwave Theor. Tech. 49 (2001) 2117.
[7] N. Setter, D. Damjanovic, L. Eng, G. Fox, S. Gevorgian, S. Hong, A. Kingon, H. Kohlstedt, N.Y. Park, G.B. Stephenson, I. Stolitchnov, A.K. Tagantsev, D.V. Taylor, T. Yamada, S. Streiffer, J. Appl. Phys. 100 (2006) 051606.
[8] J. Lu, S. Schmidt, D.S. Boesch, N. Pervez, R.A. York, S. Stemmer, Appl. Phys. Lett. 88 (2006) 112905.
[9] M.H. Kwak, S.E. Moon, S-J. Lee, Y.T. Kim, H-C. Ryu, W-J. Kim, Integr. Ferroelectr. 54 (2003) 659.
[10] K. Bethe, Philips Res. Rep. 25 (1970) 2.
[11] S. Gevorgian, A. Vorobiev, T. Lewin, J. Appl. Phys. 99 (2006) 124112.
[12] B. Panda, A. Roy, A. Dhar, S.K. Rayb, J. Appl. Phys. 101 (2007) 064116.
[13] I.P. Koutsaroff, A. Kassam, M. Zelner, P. Woo, L. McNeil, T. Bernacki, A. Cervin-Lawry, A. Patel, Mater. Res. Soc. Symp. Proc. (MRS) 748 (2003) U6.1.1.
[14] R.W. Hoffman, Thin Solid Films 34 (1976) 185.
[15] J.-P. Maria, C.B. Parker, A.I. Kingon, G. Stauf, IEEE International Symposium on Applications of Ferroelectrics (ISAF), 2002, p. 151.
[16] J. Nath, W.M. Fathelbab, P.G. Lam, D. Ghosh, S. Aygün, K.G. Gard, J.-P. Maria, A.I. Kingon, M.B. Steer, IEEE MTT-S International Microwave Symposium Digest (2006) 552.
[17] D. Ghosh, B. Laughlin, J. Nath, A.I. Kingon, M.B. Steer, J.-P. Maria, Thin Solid Films 496 (2006) 669.
[18] Z. Ma, A.J. Becker, P. Polakos, H. Huggins, J. Pastalan, H. Wu, K. Watts, Y.H. Wong, P. Mankiewich, IEEE Trans. Microw. Theory Techn. 45 (1998) 1811.
[19] E. Lifshin, Publisher: Wiley-VCH, ISBN 3527296573, 9783527296576, (1999).
[20] J.I. Langford, A.J.C. Wilson, J. Appl. Crystallogr. 11 (1978) 102.
[21] B.E. Warren, Publisher: Addison-Wesley, ISBN 0-486-66317-5, (1969).
[22] I.P. Koutsaroff, P. Woo, L. McNeil, M. Zelner, A. Kassam, M. Capanu, L. Chmiel, B. McClelland, A. Cervin-Lawry, IEEE International Symposium on Applications of Ferroelectrics (ISAF), 2002, p. 247.
[23] A. Ioachim, M.I. Toacsan, M.G. Banciu, L. Nedelcu, C.A. Dutu, F. Sava, M. Popescu, N. Scarisoreanu, M. Dinescu, International Semiconductor Conference 2 (2006) 271.
[24] A. Ioachim, H.V. Alexandru, C. Berbecaru, S. Antohe, F. Stanculescu, M.G. Banciu, M.I. Toacsen, L. Nedelcu, D. Ghetu, A. Dutu, G. Stoica, Mater. Sci. Eng., C 26 (2006) 1156.
[25] M. Klee, D. Wissen, W. Keur, R. Kiewitt, D. Bausen, P. Lok, Mater. Res. Soc. Symp. Proc. (MRS) 655 (2001) CC13.1.1.
[26] C.B. Parker, J.-P. Maria, A.I. Kingon, Appl. Phys. Lett. 81 (2002) 340.
[27] R. Thomas, V.K. Varadan, S. Komameni, D.C. Dube, J. Appl. Phys. 90 (2001) 1480.
[28] A.K. Jonscher, J. Phys., D, Appl. Phys. 32 (1999) R57.
[29] Y. Fukuda, K. Numata, K. Aoki, A. Nishimura, Jpn. J. Appl. Phys. 35 (1996) 5178.
[30] J.D. Baniecki, R.B. Laibowitz, T.M. Shaw, P.R. Duncombe, D.A. Neumayer, D.E. Kotecki, H. Shen, Q.Y. Ma, Appl. Phys. Lett. 72 (1998) 498.
[31] M.P.J. Tiggelman, K. Reimann, J. Liu, M. Klee, W. Keur, R. Mauzock, J. Schmitz, R.J.E. Hueting, IEEE International Conference on Microelectronic Test Structures, 2008, p. 190.
[32] I.P. Koutsaroff, T. Bernacki, M. Zelner, A. Cervin-Lawry, A. Kassam, P. Woo, L. Woodward, A. Patel, Mater. Res. Soc. Symp. Proc. (MRS) 784 (2004) 319.